

Modification using additional NaOH for the preparation of γ -Fe₂O₃ nanoparticles by chemically induced transition

Hong Mao¹, Jian Li¹, Longlong Chen¹, Yueqiang Lin¹, Xiaodong Liu¹, Junming Li¹, Xiaomin Gong¹, Decai Li²

¹School of Physical Science and Technology, Southwest University, Chongqing 400715, People's Republic of China

²School of Mechanical and Control Engineering, Beijing Jiaotong University, Beijing 100044, People's Republic of China
E-mail: aizhong@swu.edu.cn

Published in Micro & Nano Letters; Received on 28th July 2014; Revised on 10th September 2014; Accepted on 18th September 2014

γ -Fe₂O₃ nanoparticles coated with a layer of FeCl₃·6H₂O were prepared by chemically induced transition in FeCl₂ solution. NaOH was added to the reaction solution, to investigate the effect of alkalinity on the resulting particles. Vibrating sample magnetometry, transmission electron microscopy, X-ray diffraction, energy-dispersive X-ray spectroscopy and X-ray photoelectron spectroscopy were used to characterise the products. Additional NaOH stimulated the epitaxial growth of γ -Fe₂O₃ on the γ -Fe₂O₃ crystallites and more FeCl₃·6H₂O adsorbed on γ -Fe₂O₃. Under the experimental conditions, the increase in γ -Fe₂O₃ content was larger than that of FeCl₃·6H₂O, at ≤ 0.7 M NaOH. At >0.7 M NaOH, the increase in γ -Fe₂O₃ content was less than that of FeCl₃·6H₂O. The non-monotonic variation of the FeCl₃·6H₂O/ γ -Fe₂O₃ ratio was consistent with this result, and was consistent with the variation in apparent specific magnetisation with increasing NaOH concentration.

1. Introduction: Nanotechnology is the understanding and control of matter at dimensions of approximately 1–100 nm, where unique phenomena enable novel applications [1]. Iron oxides have attracted much attention, because of their interesting electronic, magnetic and catalytic properties. They have potential in electro-optical materials, sorbents, pigments, ion exchange, magnetic response imaging and catalysis [2]. Magnetite (Fe₃O₄) and maghemite (γ -Fe₂O₃) are widely used as ferromagnetic materials. Magnetic nanoparticles with diameters <100 nm, such as those of Fe₃O₄ and γ -Fe₂O₃, have attracted increasing interest. They potentially allow magnetic ordering phenomena in materials with reduced dimensions to be investigated, and may lead to new technologies [3–5]. Most magnetic nanoparticle studies have focused on developing syntheses [1, 6]. Liquid-phase synthesis is often used to prepare inorganic nanoparticles [7]. The conventional aqueous synthesis of γ -Fe₂O₃ particles involves three or more steps [8]. We previously prepared γ -Fe₂O₃ nanoparticles by treating a FeOOH/Mg(OH)₂ precursor with FeCl₂ solution. The precursor was synthesised by co-precipitation, and the nanoparticles were subsequently prepared by chemically induced transition [9, 10]. Such nanoparticles have been applied as ferrofluids [11], nanoparticle mimetic enzymes [12] and nanoparticle films [13].

During the above-mentioned synthesis of γ -Fe₂O₃ nanoparticles from FeOOH/Mg(OH)₂, FeOOH transformed into γ -Fe₂O₃ nanoparticles, and Mg(OH)₂ dissolved [9]. Alkaline solution generally assists this precipitation reaction. Here, NaOH solution was added to the treatment solution. The dependence of apparent magnetisation on the particle microstructure was revealed. The effect of alkalinity on the magnetic nanoparticles prepared by chemically induced transition was investigated.

2. Experimental

2.1. Preparation: The precursor was synthesised by the co-precipitation of FeCl₃ and Mg(NO₃)₂ [9]. The precursor was added to the FeCl₂ solution (0.25 M, 400 ml), which was then refluxed for 20 min. Twenty millilitres of NaOH solution of the specific concentration was then added to the boiling FeCl₂ solution, and the resulting mixture was refluxed for 10 min. The mixture was allowed to cool to room temperature, and the particles were allowed to settle. NaOH concentrations of 0.3, 0.7, 1.4, 2.0 and

3.0 M were used to prepare samples (1), (2), (3), (4) and (5), respectively. Unmodified particles were also prepared by adding the precursor to FeCl₂ solution and refluxing for 30 min, giving sample (0).

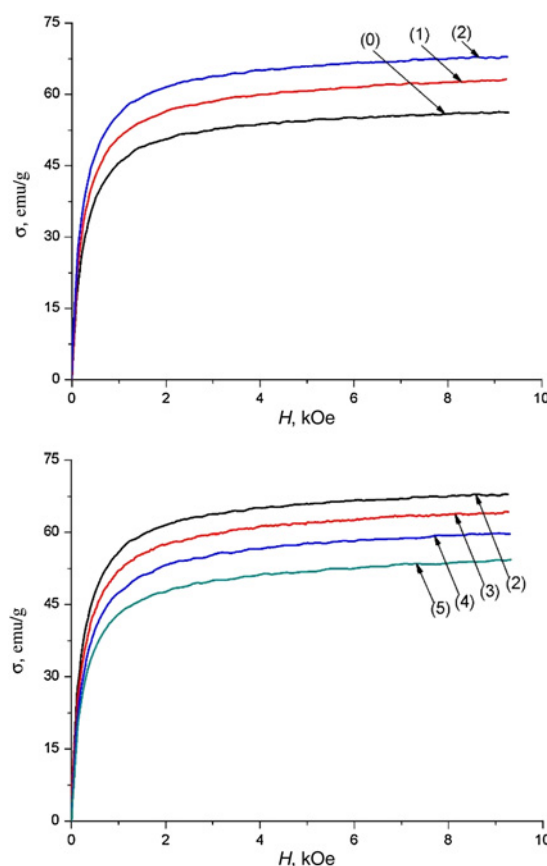
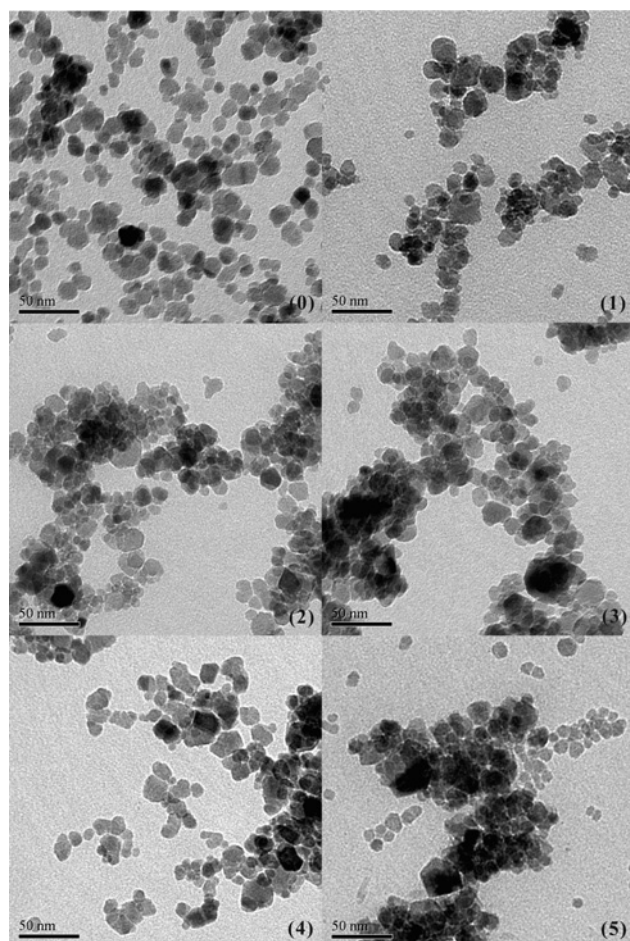
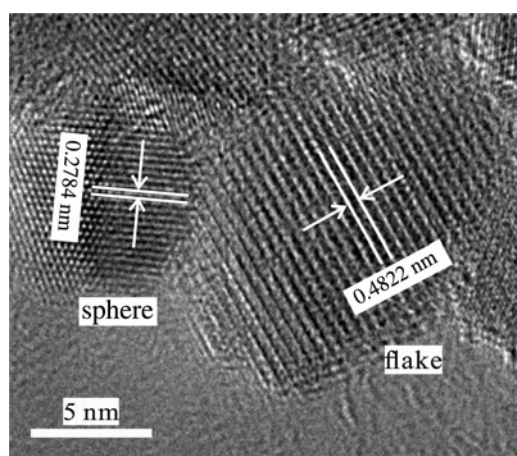
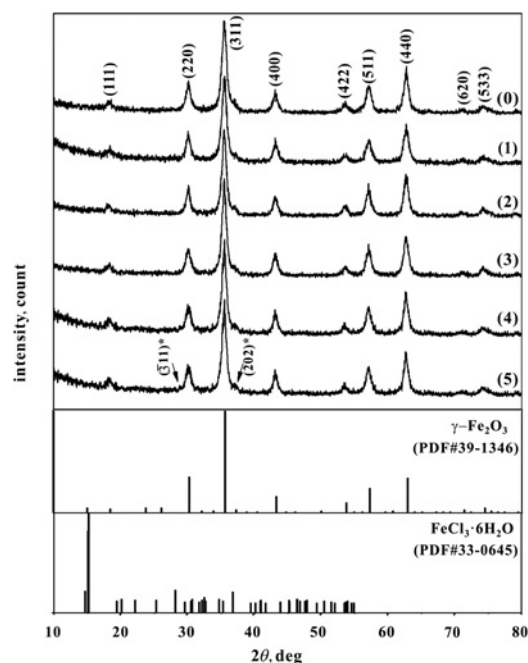


Figure 1 Specific magnetisation curves of the samples

Table 1 Specific saturation magnetisations (σ_s) and grain sizes (d_c)

Sample	σ_s , emu/g	d_c , nm
(0)	57.71	9.1
(1)	66.32	9.4
(2)	71.49	9.6
(3)	68.67	10.2
(4)	60.86	10.6
(5)	56.43	10.8

**Figure 2** Representative TEM images of the samples**Figure 3** HRTEM images of the spherical and flake-shaped nanoparticles**Figure 4** XRD patterns of the samples, with (hkl) and (hkl)* corresponding to $\gamma\text{-Fe}_2\text{O}_3$ and $\text{FeCl}_3 \cdot 6\text{H}_2\text{O}$, respectively

2.2. Characterisation: Curves of the specific magnetisation (σ) against field strength (H) were measured by vibrating sample magnetometry (VSM; HH-15). Particle morphologies were observed by transmission electron microscopy (TEM; Tecnai, G20ST). Crystal structures were analysed by high-resolution TEM (HRTEM; JEM-2100F) and X-ray diffraction (XRD; D/Max-RC). Bulk and surface chemical compositions were analysed by energy-dispersive X-ray spectroscopy (EDX; Genesis) and X-ray photoelectron spectroscopy (XPS; XSAM800), respectively.

3. Results and analysis: Fig. 1 shows plots of σ against H for the samples. All samples were ferromagnetic, with σ varying non-monotonically with increasing NaOH. σ initially increased with the increasing NaOH concentration from 0 (sample (0)) to 0.7 M (sample (2)), and then decreased with further increase from 0.7 (sample (2)) to 3.0 M (sample (5)). Specific saturation magnetisations (σ_s) were deduced by plotting σ against $1/H$ in the high-field region [14], and are listed in Table 1.

TEM images of the samples are shown in Fig. 2. Sample (0) consisted of nearly spherical nanoparticles. Statistical analysis [15] indicated the particle size obeyed a lognormal distribution, and had a median diameter of 9.92 nm and the standard deviation of 0.29. Images of samples (1)–(5) showed that they consisted of irregular flake particles and nearly spherical particles.

Table 2 Atomic percentages (a_i) of O, Fe and Cl from EDX and XPS measurements

Sample	EDX			XPS		
	O	Fe	Cl	O	Fe	Cl
(0)	50.80	47.86	1.34	71.52	25.75	2.73
(1)	49.70	48.94	1.36	73.22	24.57	2.21
(2)	48.27	50.51	1.22	73.17	24.83	2.00
(3)	50.77	48.05	1.18	72.26	24.53	2.21
(4)	50.18	48.14	1.68	73.94	24.45	2.61
(5)	45.03	52.02	2.95	72.69	23.29	4.02

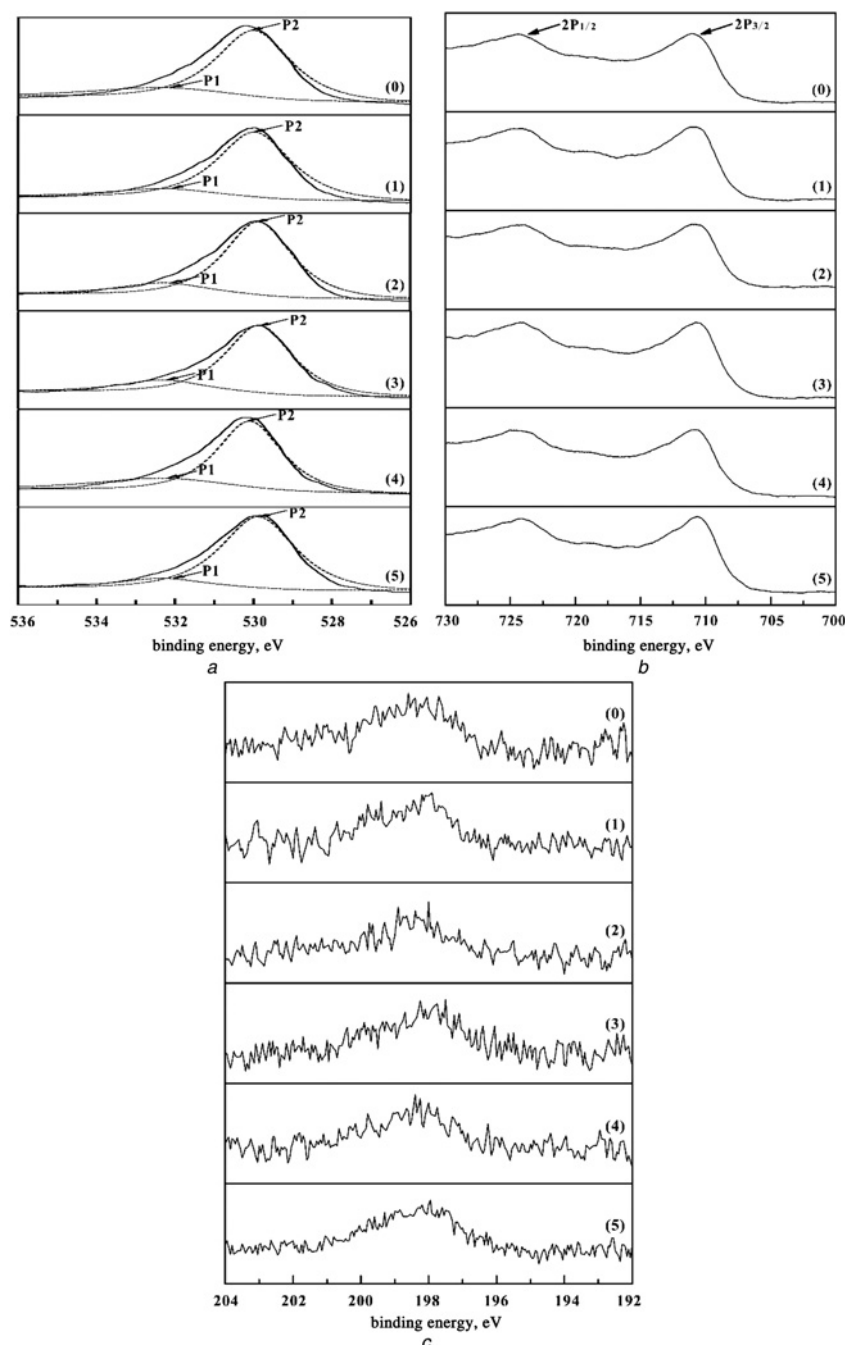


Figure 5 XPS results for O 1s lines (Fig. 5a), Fe 2p lines (Fig. 5b) and Cl 2p lines (Fig. 5c)

HRTEM revealed that both particle types were single crystalline (Fig. 3). XRD patterns of the samples (Fig. 4) revealed that they were predominantly γ -Fe₂O₃ with trace FeCl₃·6H₂O. The grain size (d_c) was estimated from the half-maximum width of the (311) diffraction peak (β) using Scherrer's formula [16]

$$d_c = k\lambda/\beta \cos \theta \quad (1)$$

where k is a constant ($k=0.89$), λ is the wavelength (CuK α wavelength of 0.1542 nm), and θ is the Bragg diffraction angle of the (311) plane. d_c increased with increasing NaOH concentration (Table 1). For sample (0), the calculated d_c was less than the size observed by TEM, which may have been because of the γ -Fe₂O₃ grains being coated by other matter.

EDX spectroscopy showed that the particles contained O, Fe and Cl, but not Mg and Na. Quantitative analysis results are listed in Table 2.

XPS confirmed that the samples contained O, Fe and Cl, but not Mg and Na. Fig. 5 shows the O 1s, Fe 2p and Cl 2p spectra of all samples. Quantitative analysis results are listed in Table 2. The observed binding energies (Table 3) indicated that γ -Fe₂O₃ and FeCl₃ were present in all samples. Oxide-binding energy data indicated the presence of H₂O [17] in the samples, which may have been because of the crystallised water in FeCl₃·6H₂O and/or adsorbed H₂O.

4. Discussion: The analyses indicated that the samples were predominantly γ -Fe₂O₃, with a small amount of FeCl₃·6H₂O. The γ -Fe₂O₃ grain size and FeCl₃ content increased with the addition

Table 3 XPS-binding energies of elements in samples (eV)

Sample	O 1s	Fe 2p _{3/2}	Cl 2p
(0)	532.30(P1)	530.00(P2)	711.11
(1)	532.30(P1)	529.98(P2)	710.99
(2)	532.28(P1)	529.87(P2)	710.96
(3)	532.30(P1)	529.86(P2)	710.97
(4)	532.30(P1)	530.10(P2)	711.01
(5)	532.32(P1)	529.88(P2)	710.77
$\gamma\text{-Fe}_2\text{O}_3$	529.50	710.90	
FeCl_3		711.30	198.80
H_2O	532.60		

Note: Standard data from the NIST X-ray Photoelectron Spectroscopy Database (www.nist.gov)

of NaOH. The $\gamma\text{-Fe}_2\text{O}_3/\text{FeCl}_3\cdot 6\text{H}_2\text{O}$ ratio of each sample was determined from the quantitative elemental analyses.

Molar percentages of the $\gamma\text{-Fe}_2\text{O}_3$ (y_γ) and FeCl_3 (y_{cl}) phases were estimated from the atomic percentages of Fe and Cl (a_{Fe} and a_{cl} ; Table 2) measured by EDX and XPS, respectively, according to

$$y = \frac{3a_{\text{Fe}} - a_{\text{cl}}}{3a_{\text{Fe}} + a_{\text{cl}}} \times 100$$

$$y_{\text{cl}} = 100 - y = \frac{2a_{\text{cl}}}{3a_{\text{Fe}} + a_{\text{cl}}} \times 100 \quad (2)$$

The mass fraction percentages of each phase (z_i) were deduced from

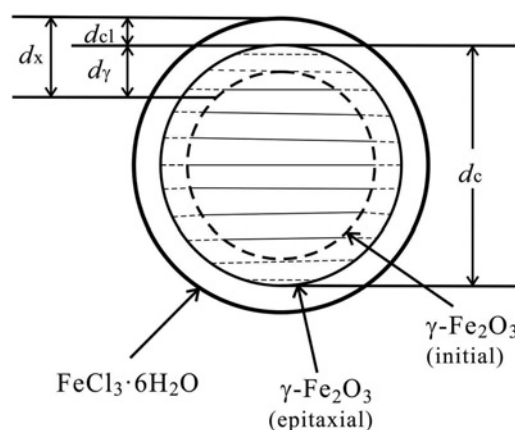
$$z_i = \frac{y_i A_i}{\sum y_i A_i \times 100} \quad (3)$$

where A_i is the molar weight of the i th phase. Accordingly, the mass fraction percentages were calculated from the values of y_i and molecular weights of $\gamma\text{-Fe}_2\text{O}_3$ and $\text{FeCl}_3\cdot 6\text{H}_2\text{O}$. The values of y_i and z_i from EDX and XPS measurements are listed in Table 4.

For each sample, the $\text{FeCl}_3\cdot 6\text{H}_2\text{O}/\gamma\text{-Fe}_2\text{O}_3$ mass ratio (z_{cl}/z_γ) obtained from EDX was much smaller than that obtained from XPS. EDX information is obtained from signal depths that largely exceed the nanoparticle dimensions, whereas XPS information is obtained from the surface to a depth of $\sim 3\lambda$ ($\lambda = 1.27$ nm for Fe 2p electrons) [18, 19]. Therefore the EDX results reflected the average z_{cl}/z_γ across the entire sample, whereas the XPS results reflected the nanoparticle surface ratio. The difference in z_{cl}/z_γ

Table 4 Molar percentages (y_i) and mass percentages (z_i) of phases determined by (a) EDX and (b) XPS

Sample	y_γ	y_{cl}	Z_γ	Z_{cl}	$Z_{\text{cl}}/Z_\gamma (\times 10^{-2})$
(a)					
(0)	98.15	1.85	96.91	3.09	3.19
(1)	98.16	1.84	96.93	3.07	3.16
(2)	98.40	1.60	97.32	2.68	2.75
(3)	98.39	1.61	97.31	2.69	2.76
(4)	97.70	2.30	96.17	3.83	3.98
(5)	96.14	3.86	93.64	6.36	6.79
(b)					
(0)	93.17	6.83	88.96	11.04	12.41
(1)	94.18	5.82	90.53	9.47	10.46
(2)	94.77	5.23	91.46	8.54	9.33
(3)	94.20	5.80	90.56	9.44	10.42
(4)	93.13	6.87	88.90	11.10	12.49
(5)	89.15	10.85	82.92	17.08	20.60

**Figure 6** Schematic representation of the particle structure as detected by XPS

between the EDX and XPS results suggested that $\text{FeCl}_3\cdot 6\text{H}_2\text{O}$ formed outside of the $\gamma\text{-Fe}_2\text{O}_3$ phase in each sample. This indicated that the precursor first transformed into $\gamma\text{-Fe}_2\text{O}_3$ nanocrystallites in the FeCl_2 solution, along with the dissolution of $\text{Mg}(\text{OH})_2$. Fe^{2+} simultaneously oxidised to Fe^{3+} , which adsorbed on the $\gamma\text{-Fe}_2\text{O}_3$ crystallites during precipitation, to form the $\text{FeCl}_3\cdot 6\text{H}_2\text{O}$ surface layer. XRD indicated that the $\gamma\text{-Fe}_2\text{O}_3$ grain size increased with increasing NaOH content. This suggested that additional NaOH stimulated the formation of an epitaxial $\gamma\text{-Fe}_2\text{O}_3$ layer on the $\gamma\text{-Fe}_2\text{O}_3$ crystallite core. A schematic of the particle structure as detected by XPS is shown in Fig. 6.

The z_{cl}/z_γ ratios determined from EDX and XPS decreased with increasing NaOH concentration at ≤ 0.7 M (samples (0)–(2), Table 4). The ratio increased with increasing NaOH concentration at > 0.7 M (samples (2)–(5), Table 4). Therefore, NaOH stimulated the epitaxial growth of $\gamma\text{-Fe}_2\text{O}_3$ at ≤ 0.7 M, and facilitated FeCl_3 formation on $\gamma\text{-Fe}_2\text{O}_3$ crystallites and the epitaxial growth of $\gamma\text{-Fe}_2\text{O}_3$ at > 0.7 M). σ varied non-monotonically with increasing NaOH concentration. This was related to the z_{cl}/z_γ ratio, which was similar to the ratio of the surface layer thickness of $\text{FeCl}_3\cdot 6\text{H}_2\text{O}$ (d_{cl}) to that of $\gamma\text{-Fe}_2\text{O}_3$ (d_γ), within the measured XPS depth (d_x) (Fig. 6). At ≤ 0.7 M NaOH, the amount of $\text{FeCl}_3\cdot 6\text{H}_2\text{O}$ was very low, resulting in a small d_{cl} upon the epitaxial growth of $\gamma\text{-Fe}_2\text{O}_3$. At > 0.7 M NaOH, the amount of $\text{FeCl}_3\cdot 6\text{H}_2\text{O}$ increased, resulting in a larger d_{cl} upon the epitaxial growth of $\gamma\text{-Fe}_2\text{O}_3$. Thus, the trends in z_{cl}/z_γ from EDX and XPS were similar. The relationship between σ and z_{cl}/z_γ was deduced as follows. The samples consisted of $\gamma\text{-Fe}_2\text{O}_3$ and $\text{FeCl}_3\cdot 6\text{H}_2\text{O}$, so σ could be described by

$$\sigma = \phi_{\text{m},\gamma} \sigma_\gamma + \phi_{\text{m},\text{cl}} \sigma_{\text{cl}} \quad (4)$$

where σ_γ and σ_{cl} are the specific magnetisations of $\gamma\text{-Fe}_2\text{O}_3$ and $\text{FeCl}_3\cdot 6\text{H}_2\text{O}$, respectively, and $\phi_{\text{m},\gamma}$ ($\phi_{\text{m},\gamma} = z_\gamma/100$) and $\phi_{\text{m},\text{cl}}$ ($\phi_{\text{m},\text{cl}} = z_{\text{cl}}/100$) are the mass fractions of $\gamma\text{-Fe}_2\text{O}_3$ and $\text{FeCl}_3\cdot 6\text{H}_2\text{O}$, respectively. According to the definition of mass fraction, $\phi_{\text{m},\gamma} + \phi_{\text{m},\text{cl}} = 1$. Thus, (4) may be written as

$$\sigma = \frac{1}{1 + \phi_{\text{m},\text{cl}}/\phi_{\text{m},\gamma}} (\sigma_\gamma - \sigma_{\text{cl}}) + \sigma_{\text{cl}} \quad (5)$$

That is

$$\sigma = \frac{1}{1 + Z_{\text{cl}}/Z_\gamma} (\sigma_\gamma - \sigma_{\text{cl}}) + \sigma_{\text{cl}} \quad (6)$$

σ_γ and σ_{cl} may be regarded as constants, with $\sigma_\gamma \gg \sigma_{\text{cl}}$. Equation (6) shows that σ is inversely related to z_{cl}/z_γ , in agreement with the experimental results (i.e. σ increased from sample (0) to (2) because of

the decreasing $z_{\text{cl}}/z_{\text{r}}$, and reduced from samples (2) to (5) because of the increasing $z_{\text{cl}}/z_{\text{r}}$.

5. Conclusion: Fe^{2+} oxidised to Fe^{3+} during the synthesis of $\gamma\text{-Fe}_2\text{O}_3$ nanoparticles by chemically induced transition in FeCl_2 solution. NaOH led to the formation of a $\gamma\text{-Fe}_2\text{O}_3$ epitaxial layer on the $\gamma\text{-Fe}_2\text{O}_3$ crystallites formed from precursor transition. Additional NaOH caused more $\text{FeCl}_3 \cdot 6\text{H}_2\text{O}$ to absorb to the $\gamma\text{-Fe}_2\text{O}_3$ grains. The apparent specific magnetisation of the samples resulted from competition between the increase in amounts of $\gamma\text{-Fe}_2\text{O}_3$ and $\text{FeCl}_3 \cdot 6\text{H}_2\text{O}$. The increase in $\gamma\text{-Fe}_2\text{O}_3$ content was larger than that of $\text{FeCl}_3 \cdot 6\text{H}_2\text{O}$, under the current conditions. This led to an increase in specific magnetisation strength with increasing NaOH concentration, at <0.7 M. When the NaOH concentration was >0.7 M, the increase in $\gamma\text{-Fe}_2\text{O}_3$ content was less than that of $\text{FeCl}_3 \cdot 6\text{H}_2\text{O}$. This led to decreasing magnetisation strength with increasing NaOH concentration. The apparent specific magnetisation depended on the ratio of $\text{FeCl}_3 \cdot 6\text{H}_2\text{O}$ to $\gamma\text{-Fe}_2\text{O}_3$, as the concentration of additional NaOH increased. During the synthesis of the $\gamma\text{-Fe}_2\text{O}_3$ nanoparticles, Fe(III) compounds could form on $\gamma\text{-Fe}_2\text{O}_3$ crystallites, in the presence of NaOH and salts of other melts. This route could potentially be used to prepare composite nanoparticles containing $\gamma\text{-Fe}_2\text{O}_3$.

6. Acknowledgment: Financial support was provided by the National Natural Science Foundation of China (grant numbers 51375039 and 11074205).

7 References

- [1] Mathew D.S., Juang R.-S.: 'An overview of the structure and magnetism of spinel ferrite nanoparticles and their synthesis in microemulsions', *Chem. Eng. J.*, 2007, **129**, (1–3), pp. 51–65
- [2] Liu X., Qiu G., Yan A., Wang Z., Li X.: 'Hydrothermal synthesis and characterization of $\alpha\text{-FeOOH}$ and $\gamma\text{-Fe}_2\text{O}_3$ uniform nanocrystallines', *J. Alloys Compd.*, 2007, **433**, (1–2), pp. 216–220
- [3] Willard M.A., Kurihara L.K., Carpenter E.E., Calvin S., Harries V.G.: 'Chemically prepared magnetic nanoparticles', *Int. Mater. Rev.*, 2004, **49**, (3–4), pp. 125–170
- [4] Laurent S., Forge D., Port M., *ET AL.*: 'Magnetic iron oxide nanoparticles: synthesis, stabilization, vectorization, physicochemical characterizations, and biological applications', *Chem. Rev.*, 2008, **108**, pp. 2064–2110
- [5] Reddy L.H., Arias J.L., Nicolas J., Coureur P.: 'Magnetic nanoparticles: design and characterization, toxicity and biocompatibility, pharmaceutical and biomedical applications', *Chem. Rev.*, 2012, **112**, (11), pp. 5818–5878
- [6] Jiang J., Yang Y.M.: 'Facile synthesis of nanocrystalline spinel NiFe_2O_4 via a novel soft chemistry route', *Mater. Lett.*, 2007, **61**, (21), pp. 4276–4279
- [7] Cushing B.L., Kolesnichenko V.L., O'Connor C.J.: 'Recent advances in the liquid-phase syntheses of inorganic nanoparticles', *Chem. Rev.*, 2004, **104**, pp. 3893–3946
- [8] Asuha S., Zhao S., Wu H.W., Sony L., Tegus O.: 'One step synthesis of maghemite nanoparticles by direct thermal decomposition of Fe-urea complex and their properties', *J. Alloys Compd.*, 2009, **472**, (1–2), pp. L23–L25
- [9] Wen B.C., Li J., Lin Y.Q., *ET AL.*: 'A novel preparation method for $\gamma\text{-Fe}_2\text{O}_3$ nanoparticles and their characterization', *Mater. Chem. Phys.*, 2011, **128**, pp. 35–38
- [10] Fu J., Lin L.H., Li J.: 'A novel preparation method for magnetic nanoparticles and their characterization'. Proc. of 2011 China Functional Materials Technology and Industry Forum (CFMTIF), Chongqing, China, 2011, pp. 46–50
- [11] Li J., Fu J., Liu Y.Q., Liu X.D., Lin L.H., Chen L.L.: 'The magneto-optical behaviors modulated by unaggregated system for $\gamma\text{-Fe}_2\text{O}_3\text{-ZnFe}_2\text{O}_4$ binary ferrofluids', *AIP Adv.*, 2012, **2**, p. 042124
- [12] Shi W.B., Zhang X.D., He S.H., Li J., Huang Y.M.: 'Fast screening of the nanoparticles-based enzyme mimetics by a chemiluminescence method', *Sci. Sin. Chim.*, 2013, **43**, (11), pp. 1591–1598 (in Chinese)
- [13] Liu Z.J., Zhang S.Y., Huo J.Q., Li J., Qiu X.Y.: 'Effect of HfO_x buffer layer on the resistive switching characteristics of $\gamma\text{-Fe}_2\text{O}_3$ nanoparticle films', *Sci. Sin. Phys. Mech. Astron.*, 2014, **44**, (4), pp. 417–424 (in Chinese)
- [14] Arulmurugan R., Vaidyanathan G., Sendhilnathan S., Jeyadevan B.: 'Co–Zn ferrite nanoparticles for ferrofluid preparation: study on magnetic properties', *Physica B*, 2005, **363**, (1–4), pp. 225–231
- [15] Granqvist C.G., Bhrman R.A.: 'Ultrafine metal particles', *J. Appl. Phys.*, 1976, **47**, pp. 2200–2219
- [16] Sato T., Iijima T., Seki M., Inagaki N.: 'Magnetic properties of ultrafine ferrite particles', *J. Magn. Magn. Mater.*, 1987, **65**, (2–3), pp. 252–256
- [17] Martensson N., Malmquist P.A., Svensson S., *ET AL.*: 'Molecular and solid water, a comparative Esca study', *J. Chem.*, 1977, **1**, pp. 191–195
- [18] Smová-šloufová I., Vlčková B., Bastel Z., Hasslett T.L.: 'Bimetallic (Ag) Au nanoparticles prepared by the seed growth method: two-dimensional assembling, characterization by energy dispersive X-ray analysis, X-ray photoelectron spectroscopy, and surface enhanced Raman spectroscopy, and proposed mechanism of growth', *Langmuir*, 2004, **20**, pp. 3407–3415
- [19] Tanuma S., Powell C.J., Penn D.R.: 'Calculations of electron inelastic mean free paths. II. Data for 27 elements over the 50–2000 eV range', *Surf. Interface Anal.*, 1991, **17**, (13), pp. 911–926